Three-Dimensional Contact Dynamic Model of the Human Knee Joint During Walking

Joung Hwan Mun*, Dae-Weon Lee

Department of Bio-Mechatronic Engineering, College of Life Science & Technology, Sungkyunkwan University, 300 Chunchun, Jangan, Suwon, Kyunggi, 440-746, Korea

It is well known that the geometry of the articular surface has a major role in determining the position of articular contact and the lines of action for the contact forces. The contact force calculation of the knee joint under the effect of sliding and rolling is one of the most challenging issues in this field. We present a 3-D human knee joint model including sliding and rolling motions and major ligaments to calculate the lateral and medial condyle contact forces from the recovered total internal reaction force using inverse dynamic contact modeling and the Least -Square method. As results, it is believed that the patella, muscles and tendon affect a lot for the internal reaction forces at the initial heel contact stage. With increasing flexion angles during gait, the decreasing contact area is progressively shifted to the posterior direction on the tibia plateau. In addition, the medial side contact force is larger than the lateral side contact force in the knee joint during normal human walking. The total internal forces of the knee joint are reasonabe compared to previous studies.

Key Words : Digital Human Model, Gait analysis, Human Motion, Kinetics, Biomechanics

1. Introduction

The human knee joint is the intermediate joint of the lower limb thatis the largest and most complex joint in the body. Understanding of joint-articulating surface motion is essential for assessment of joint wear, stability, mobility, degeneration, determination of proper diagnosis and surgical treatment of joint disease. The articular geometry of the tibiofemoral condyle and the surrounding capsule ligamentous constraints lead the articular surface motion of the knee joint during motion. The functionality of the knee joint cannot be accurately modeled without considering the effects of sliding and rolling motions. The kinematics of the joint cannot be modeled as a point contact, a hinge joint as one degrees-of-freedom (DOF), universal joint (two DOF) or spherical joint (three DOF) but has to take into consideration both sliding and rolling motions. Indeed, many studies have addressed this joint using a single point-of-contact with two or three degrees-of-freedom (Kadaba et al., 1990; Bobbert et al., 1991; Bronzion, 1995; Allard et al., 1995; Reinschmidt et al., 1997; Attfield et al., 1998; Zwick et al., 2002) or by using two spherically shaped balls with fixed radii (Wilson and O'Connor, 1997; Abdel-Rahman and Hefzy, 1998). These models are faced with difficulties because of the computational complexity and equation formulation resulting from the complex geometry of the articular joint in the knee. The redundancy of muscles and ligaments led to further complications.

The contact force calculation for the knee joint considering the effect of sliding and rolling is one of the most challenging issues in this field. In order to calculate contact forces in the knee joint

* Corresponding Author,
E-mail : jmun@skku.ac.kr
TEL : +82-31-290-7827; **FAX** : +82-31-290-7830
Department of Bio-Mechatronic Engineering, College of Life Science & Technology, Sungkyunkwan University 300 Chunchun, Jangan, Suwon, Kyunggi, 440-746, Korea. (Manuscript **Received** April 7, 2003; **Revised** December 16, 2003)

in three-dimensional analysis (3D), two different approaches have been attempted : (1) is based on the depth of penetration (Eberhardt et al., 1990 ; 1991 ; Ateshian et al., 1994) of the joint and (2) is based on a Quasi-static equilibrium (Wilson and O'connor, 1997 ; Abdel-Rahman and Hefzy, 1998 ; Mun and Takeuchi, 2002). Although these two methods are conceptually identical, inverse dynamics due to human motion are different because of the input errors mainly due to skin movement in gait. The lateral and medial side knee joint distance change of the contact point between femoral condyles and tibia surface during one gait cycle is about 6 mm. and 19 mm., respectively (Mun, 2001). Since the Elastic modulus (E) for the cortical bone is 6900 MNm^{-2} (Brown et al., 1984), penetration/separation-based method is inadequate for gait analysis.

Wilson and O'connor (1997) reported a three dimensional geometric model of the knee joint in gait analysis to predict the kinematics of the knee from the geometry of its anatomical structures. They addressed two important problems related to the knee joint biomechanics such as the determination of the changing axis of rotation, and prediction of the lines of force through the major ligaments and femoral articulated surface. However, the geometric model they used was composed of rigid spherical surfaces that include much error in prediction the position and lines of action of the contact forces. Furthermore, kinematic locking occurred for joint angles greater than 60 degree due to the geometric simplification.

More recently, Abdel-Rahman and Hefzy (1998) presented a 3D human knee joint model undergoing impact loading. The model was composed of two-body segments, the femur and tibia, in contact, with the joint ligaments represented as nonlinear elastic springs. Major limitations of the model is that first, the external force applied on the tibia is a sinusoidal impacting load that is not applicable for general 3D human locomotion. Thus, the computational model they developed cannot be applicable for understanding more standard activities where dynamic axial compressive forces act on the joint such as gait. Second, the medial and lateral articular surfaces were approximated as parts of spheres. However, since the geometry of the articular surface plays a major role in the kinematic and kinetic analysis of the dynamic knee joint model, more detailed geometry should be considered.

The objects of this study are : (1) to demonstrate a new knee joint model considering sliding, spinning and rolling motion and major ligaments to recover the total internal reaction forces at the human knee joint during gait using inverse dynamic and contact modeling and, (2) to calculate the lateral and medial condyle contact forces from the recovered total internal reaction force using the Least-square method.

2. Methods

In this study, the articular geometry was more accurately represented using two cam profiles obtained from the extrusion of the sagittal plain view of a representative Computerized Tomography (CT) image of the knee (Mun and Takeuch, 2002) as shown in Fig. 1. Also, the experimental data set, error mainly due to the skin movement during gait was reduced in the reasonable range of error employing the previously reported statistical data reduction method (Mun, 2001), was adopted for the force recovery of the invariable knee joint.

2.1 Kinematics of the knee joint contact model

We introduce a model of the human knee joint that can account for four possible contacts (one

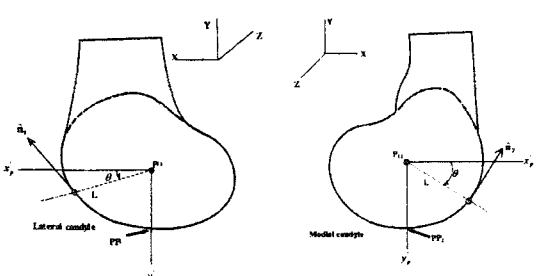

Fig. 1 The coordinate system of the digitized lateral and medical condyle contact points

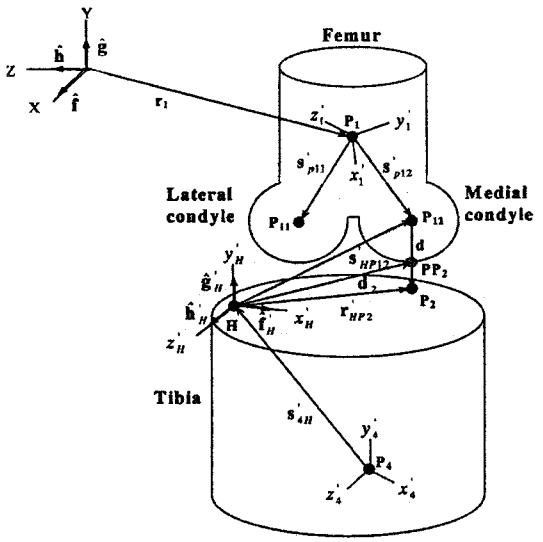

Fig. 2 The configuration of the knee Joint contact model

and two point contacts, separation, and penetration). Our model is a 6 DOF knee joint represented by two digitized cam profile spheres considering sliding and rolling as shown in Fig. 2 with major ligaments as illustrated in Figs. 6 and 7.

We briefly present the kinematic analysis needed to perform the force and torque recovery. Detailed kinematic analysis is presented on the previous report (Mun and Takeuchi, 2002). In the computational model, since the possibility of penetration and separation of the tibiofemoral joint while in motion is allowed, the system of constraint equation is assembled by only driving constraints as

$$\Phi(\mathbf{q}, t)=\lfloor \Phi^D(\mathbf{q}, t) \rfloor_{nc}=0 \tag{1}$$

With a maximal set of Cartesian generalized coordinate, $\mathbf{q}=\{x_1, y_1, z_1, x_2, y_2, z_2, x_3, y_3, z_3, x_4, y_4, z_4, x_5, y_5, z_5, x_6, y_6, z_6\}^T$, the system of driving constraint equations are

$$\Phi_1^D=\begin{Bmatrix} x_1-x_1^* \\ y_1-y_1^* \\ z_1-z_1^* \end{Bmatrix}=0 \tag{2}$$

$$\Phi_2^D=\begin{Bmatrix} x_2-x_2^* \\ y_2-y_2^* \\ z_2-z_2^* \end{Bmatrix}=0 \tag{3}$$

$$\Phi_3^D=\begin{Bmatrix} x_3-x_3^* \\ y_3-y_3^* \\ z_3-z_3^* \end{Bmatrix}=0 \tag{4}$$

$$\Phi_4^D=\begin{Bmatrix} x_4-x_4^* \\ y_4-y_4^* \\ z_4-z_4^* \end{Bmatrix}=0 \tag{5}$$

$$\Phi_5^D=\begin{Bmatrix} x_5-x_5^* \\ y_5-y_5^* \\ z_5-z_5^* \end{Bmatrix}=0 \tag{6}$$

$$\Phi_6^D=\begin{Bmatrix} x_6-x_6^* \\ y_6-y_6^* \\ z_6-z_6^* \end{Bmatrix}=0 \tag{7}$$

where $\mathbf{P}_1(x_1, y_1, z_1)$, $\mathbf{P}_2(x_2, y_2, z_2)$ and $\mathbf{P}_3(x_3, y_3, z_3)$ represent maker positions on femur and $\mathbf{P}_4(x_4, y_4, z_4)$, $\mathbf{P}_5(x_5, y_5, z_5)$ and $\mathbf{P}_6(x_6, y_6, z_6)$ are the marker positions on tibia, and all the * values are the kinematic values recovered from cubic spline functions.

In Fig. 2, the vector position of the center of two spheres $\mathbf{P}_{11}$ and $\mathbf{P}_{12}$ can be expressed in terms of the global Cartesian reference coordinate system as

$$\mathbf{P}_{11}=\mathbf{r}_1+\mathbf{A}_1\mathbf{s}'_{p11} \tag{8}$$

$$\mathbf{P}_{12}=\mathbf{r}_1+\mathbf{A}_1\mathbf{s}'_{p12} \tag{9}$$

$\mathbf{r}_1$ is the vector from the origin of the global laboratory reference to the local origin of femur segment and $\mathbf{A}_1$ is the transformation matrix from the local coordinate system of the femur to the global coordinated system during the motion. The constant local vectors $\mathbf{s}'_{p11}$ and $\mathbf{s}'_{p12}$ are calculated from the calibration stage data as

$$\mathbf{s}'_{p11}=\mathbf{A}_{1s}^{-1}(\mathbf{r}_1-\mathbf{P}_{11}) \tag{10}$$

$$\mathbf{s}'_{p12}=\mathbf{A}_{1s}^{-1}(\mathbf{r}_1-\mathbf{P}_{12}) \tag{11}$$

where $\mathbf{A}_{1s}^{-1}$ is the inverse matrix of the transformation matrix $\mathbf{A}_{1s}$ calculated at the calibration data set.

Since the geometry of contact area do major role to determine the lines of action of the forces, internal reaction force and moment and the position and orientation of the axis of rotation of the knee, the irregular shape of the outline of contacting bodies such as femoral condyle must be described numerically to get relatively accurate

results. The real geometry of the femoral condyle is that the radii of curvature increase regularly posero-anteriorly, i.e. from 17 to 38 mm. for the medial condyle and from 12 to 60 mm. for the lateral condyle. The spiral does not have only one center but a series of centers lying on a spiral. Therefore the curve of the condyles represents a spiral of a spiral (Kapandji, 1970). In order to describe the lateral and medial condyle in a closed-form expression, a cubic interpolation spline function is used.

In the computational model, the spring elements representing the ligamentous structures were assumed to be line elements extending from the femoral origin to the tibial insertion and to carry load only when they are in tension, that their length is larger than initial unstrained length L_0. Ligaments exhibit two-piece force-elongation relationship, nonlinear force-elongation in the initial stage of ligament strain and then linear force-elongation in later stages. Thus the magnitude of the force in the ith ligamentous element is expressed as;

$$F_i=\begin{cases}0; & \varepsilon_i\le 0\\ A_i(L-L_{0i})^2; & 0=\varepsilon_i\le 2\varepsilon_1\\ B_i\{L-(1+\varepsilon_1)L_{0i}\}; & \varepsilon_i\ge 2\varepsilon_1\end{cases} \quad (12)$$

where i is the strain in the ith elements, A_i and B_i are the stiffness coefficients of the ith spring element for the nonlinear and linear regions, respectively, and L and L_{0i} are its current and slack lengths, respectively. The linear range threshold is specified as $\varepsilon_1=0.03$. Values of the stiffness coefficients of the spring element employed in the model are given in Table 1. Detailed local coordinates and material properties of the ligament structures of the present model are estimated according to the previous published literature (Abdel-Rahman & Hefzy, 1998). The employed ligaments at the knee joint are shown in Figs. 6 and 7.

2.2 Force and torque recovery

In our computational knee joint model, the total internal reaction forces of the knee joint are composed of 14 components including the lateral and medial contact forces and 12 ligaments.

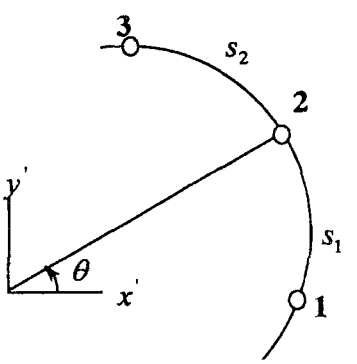

Fig. 3 Two cubic polynomials

Table 1 Local attachment coordinates and material properties of the ligamentous structures of the present model

	Local coordinates of femoral attachments			Local coordinates of tibial attachments			A_i (Nmm^{-1})	B_i (Nmm^{-1})	ε(at full extension)
	x(mm)	y(mm)	z(mm)	x'(mm)	y'(mm)	z'(mm)			
ACC	7.25	−15.6	21.25	−7.0	5.0	211.25	85.15	22.48	1.00
PAC	7.25	−20.3	19.55	2.0	2.0	212.25	83.15	26.27	1.051
APC	−4.75	−11.2	14.06	5.0	−30.0	206.25	125.0	31.26	1.004
PPC	−4.75	−23.2	15.65	−5.0	−30.0	206.25	60.0	19.29	1.05
AMC	−34.75	−1.0	26.25	−20.0	4.0	171.25	91.25	10.0	0.94
OMC	−34.75	−8.0	24.25	−35.0	−30.0	199.25	27.86	5.0	1.031
DMC	−34.75	−5.0	21.25	35.0	0.0	199.25	21.07	5.0	1.049
LCL	35.25	−15.0	21.25	45.0	−25.0	176.25	72.22	10.0	1.05
MCAP	−24.75	−38.0	6.25	−25.0	−25.0	181.25	52.59	12.0	1.08
LCAP	25.25	−35.5	8.25	25.0	−25.0	181.25	54.62	12.0	1.08
OLP	25.25	−35.5	8.25	−25.0	−25.0	181.25	21.42	3.0	1.08
APL	−24.75	−38.8	6.25	25.0	−25.0	181.25	20.82	3.0	1.07

Figure 4 shows the free body diagram of the tibia, where $\mathbf{F}_1$ is the external force from the force plate at the force center, and F_2, T_2, a_2, and α are mass related force, torque, linear acceleration and angular acceleration at the mass center of the shank segment, respectively. The internal forces F_3 and T_3 are calculated from the knee joint using a quasi-static assumption. In Fig. 4, vector variables are known except F_3 and T_3.

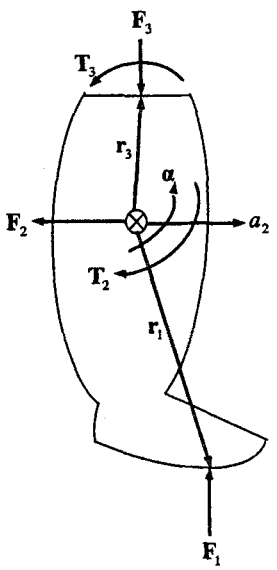

Fig. 4 The free-body diagram of the tibia

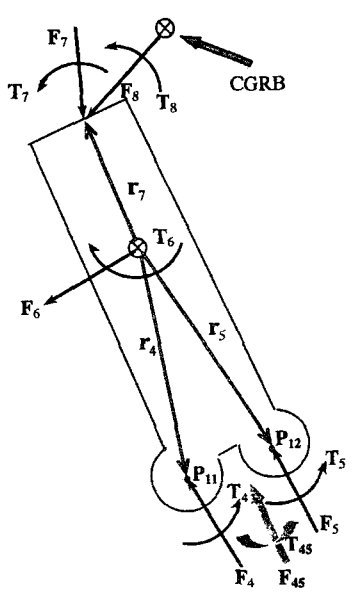

Fig. 5 The free-body diagram of the femur

The free body diagram of the femur is shown in Figure 5 where P_{11} and P_{12} are the center position of the lateral condyle and medial condyle, respectively and F_4, T_4, F_5, and T_5 are the internal reaction forces at the knee joint. We denote the terms F_6 and T_6 to be produced by the gravity and F_7 and T_7 are internal forces at the hip joint. The external force due to total mass is represented by F_8 and T_8. This is a redundant system, thus, F_{45} and T_{45} are used instead of F_4, F_5, T_4 and T_5 at the knee center. F_{45} and T_{45} are obtained from the calculated F_3 and T_3. In the Fig. 5, CGRB is the center of gravity of the human in the computational model.

Our goal is to determine the lateral and medial condyle contact forces from the total internal forces of the knee joint and twelve ligaments' reaction forces. We first develop the equilibrium equations of the tibiofemoral knee joint system as

$$F_x=\mathbf{F}^{Lc}\hat{\mathbf{n}}_x^L+\mathbf{F}^{Mc}\hat{\mathbf{n}}_x^M+\sum_{i=1}^{12}\mathbf{F}_i^{Liga}\mathbf{n}_{ix}^{Liga}-F_x^*=0 \quad (13)$$

$$F_y=\mathbf{F}^{Lc}\hat{\mathbf{n}}_y^L+\mathbf{F}^{Mc}\hat{\mathbf{n}}_y^M+\sum_{i=1}^{12}\mathbf{F}_i^{Liga}\mathbf{n}_{iy}^{Liga}-F_y^*=0 \quad (14)$$

$$F_z=\mathbf{F}^{Lc}\hat{\mathbf{n}}_z^L+\mathbf{F}^{Mc}\hat{\mathbf{n}}_z^M+\sum_{i=1}^{12}\mathbf{F}_i^{Liga}\mathbf{n}_{iz}^{Liga}-F_z^*=0 \quad (15)$$

and for the generalized moment equations as

$$M_x=\mathbf{M}^{Lc}\hat{\mathbf{n}}_x^L+\mathbf{M}^{Mc}\hat{\mathbf{n}}_x^M+\sum_{i=1}^{12}\mathbf{M}_i^{Liga}\hat{\mathbf{n}}_{ix}^{Liga}-M_x^*=0 \quad (16)$$

$$M_y=\mathbf{M}^{Lc}\hat{\mathbf{n}}_y^L+\mathbf{M}^{Mc}\hat{\mathbf{n}}_y^M+\sum_{i=1}^{12}\mathbf{M}_i^{Liga}\hat{\mathbf{n}}_{iy}^{Liga}-M_y^*=0 \quad (17)$$

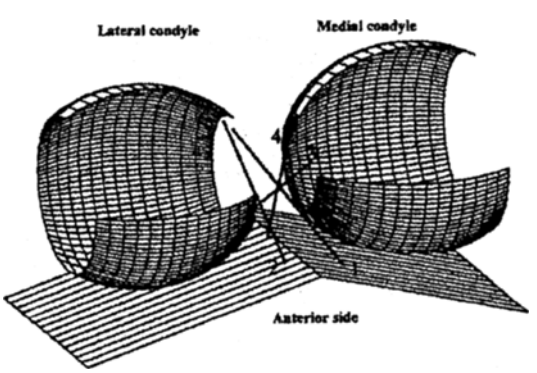

Number 1 : Anterior fibers of the Anterior Cruciate (AAC)
Number 2 : Posterior fibers of the Anterior Cruciate (PAC)
Number 3 : Anterior fibers of the Posterior Cruciate (APC)
Number 4 : Posterior fibers of the Posterior Cruciate (PPC)

Fig. 6 Cruciate ligaments at the knee joint

$$M_z=\mathbf{M}^{Lc}\hat{\mathbf{n}}_z^L+\mathbf{M}^{Mc}\hat{\mathbf{n}}_z^M+\sum_{i=1}^{12}\mathbf{M}_i^{Liga}\hat{\mathbf{n}}_{iz}^{Liga}-M_z^*=0 \quad (18)$$

where $\mathbf{F}^{Lc}$, $\mathbf{M}^{Lc}$, $\mathbf{F}^{Mc}$, $\mathbf{M}^{Mc}$, $\mathbf{F}_i^{Liga}$ and $\mathbf{M}_i^{Liga}$ are the lateral condyle contact force and moment, the medial condyle contact force and moment, and sum of the 12 ligament forces and moments, respectively and where $\hat{\mathbf{n}}$ represents the direction vectors determined from the kinematics of the contact model, and $\mathbf{F}^*$ and $\mathbf{M}^*$ are the total force and moment at the knee joint recovered from the quasi-static solution of the free-body diagram.

In order to solve this system, a *least squares method* is used. The residuals for each equation can be written as

$$\mathbf{e}=\begin{Bmatrix}\mathbf{F}-\mathbf{F}^*\\ \mathbf{M}-\mathbf{M}^*\end{Bmatrix}_{6\times1} \quad (19)$$

where $\mathbf{F}$ and $\mathbf{M}$ are the total contact force and moment of the tibiofemoral knee joint system obtained experimentally and represented as

$$\mathbf{F}=\mathbf{F}^{Lc}\hat{\mathbf{n}}^L+\mathbf{F}^{Mc}\hat{\mathbf{n}}^M+\sum_{i=1}^{12}\mathbf{F}_i^{Liga} \quad (20)$$

$$\mathbf{M}=\mathbf{r}^L\times\mathbf{F}^{Lc}\hat{\mathbf{n}}^L+\mathbf{r}^M\times\mathbf{F}^{Mc}\hat{\mathbf{n}}^M+\sum_{i=1}^{12}\mathbf{r}_i^{Liga}\times\mathbf{F}_i^{Liga} \quad (21)$$

$$\mathbf{M}=\mathbf{F}^{Lc}\tilde{\mathbf{r}}^L\hat{\mathbf{n}}^L+\mathbf{F}^{Mc}\tilde{\mathbf{r}}^M\hat{\mathbf{n}}^M+\sum_{i=1}^{12}\mathbf{F}_i^{Liga}\tilde{\mathbf{r}}_i^{Liga}\hat{\mathbf{n}}_i^{Liga} \quad (22)$$

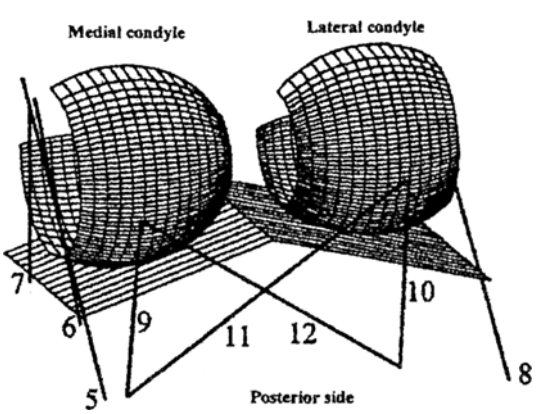

Number 5 : Anterior fibers of the Medial Collateral (AMC)
Number 6 : Oblique fibers of the Medial Collateral (OMC)
Number 7 : Deep fibers of the Medial Collateral (DMC)
Number 8 : Lateral Collateral (LCL)
Number 9 : Medial fibers of the posterior Capsule (MCAP)
Number 10 : Lateral fibers of the posterior Capsule (LCAP)
Number 11 : Oblique Popliteal Ligament (OPL)
Number 12 : Arcuate Popliteal Ligament (APL)

Fig. 7 Capsular ligaments at the knee joint

where, $\mathbf{r}^L$ and $\mathbf{r}^M$ represent vectors from the origin of the knee joint center to lateral and medical contact point during gait, respectively. Thus, the system is composed of six equations and two unknowns, namely $\mathbf{F}^{Lc}$ and $\mathbf{F}^{Mc}$.

The least-square criterion specifies that e_i be chosen to minimize the sum of the squares of the residuals, that is

$$\text{Minimize } \sum_{i=1}^{6}e_i^Te_i \quad (23)$$

The goal is to minimize e_i^2 and it requires for $i=1, \cdots, 6$ that the partial derivatives be set to zero as

$$\frac{\partial(\mathbf{e}^T\mathbf{e})}{\partial\mathbf{F}^{Lc}}=2\mathbf{e}^T\frac{\partial\mathbf{e}}{\partial\mathbf{F}^{Lc}}=0 \quad (24)$$

$$\frac{\partial(\mathbf{e}^T\mathbf{e})}{\partial\mathbf{F}^{Mc}}=2\mathbf{e}^T\frac{\partial\mathbf{e}}{\partial\mathbf{F}^{Mc}}=0 \quad (25)$$

Taking the partial derivative of Eqs. (20) and (22) with respect to unknown contact force, $\mathbf{F}^{Lc}$ and $\mathbf{F}^{Mc}$, four simultaneous linear equations are obtained as

$$\frac{\partial\mathbf{F}}{\partial\mathbf{F}^{Lc}}=\hat{\mathbf{n}}^L \quad (26)$$

$$\frac{\partial\mathbf{F}}{\partial\mathbf{F}^{Mc}}=\hat{\mathbf{n}}^M \quad (27)$$

$$\frac{\partial\mathbf{M}}{\partial\mathbf{F}^{Lc}}=\tilde{\mathbf{r}}^L\hat{\mathbf{n}}^L \quad (28)$$

$$\frac{\partial\mathbf{M}}{\partial\mathbf{F}^{Mc}}=\tilde{\mathbf{r}}^M\hat{\mathbf{n}}^M \quad (29)$$

where, $\hat{\mathbf{n}}^L$ and $\hat{\mathbf{n}}^M$ represent the direction vectors of the lateral condyle and medial condyle determined from the kinematics of the contact model, respectively. $\tilde{\mathbf{r}}^L$ and $\tilde{\mathbf{r}}^M$ is a 3×3 antisymmetric matrix that is formed from the components of $\mathbf{r}^L$ and $\mathbf{r}^M$, respectively. Thus, Eq. (19) can be rewritten as

$$\begin{bmatrix}\mathbf{F}-\mathbf{F}^*\\ \mathbf{M}-\mathbf{M}^*\end{bmatrix}^T\begin{Bmatrix}\hat{\mathbf{n}}^L\\ \tilde{\mathbf{r}}^L\hat{\mathbf{n}}^L\end{Bmatrix}=0 \quad (30)$$

$$\begin{bmatrix}\mathbf{F}-\mathbf{F}^*\\ \mathbf{M}-\mathbf{M}^*\end{bmatrix}^T\begin{Bmatrix}\hat{\mathbf{n}}^M\\ \tilde{\mathbf{r}}^M\hat{\mathbf{n}}^M\end{Bmatrix}=0 \quad (31)$$

Substituting Eqs. (30) and (31) into Eqs. (24) and (25), there exist 2 equations and 2 unknown contact forces as shown in the Eq. (32). Thus,

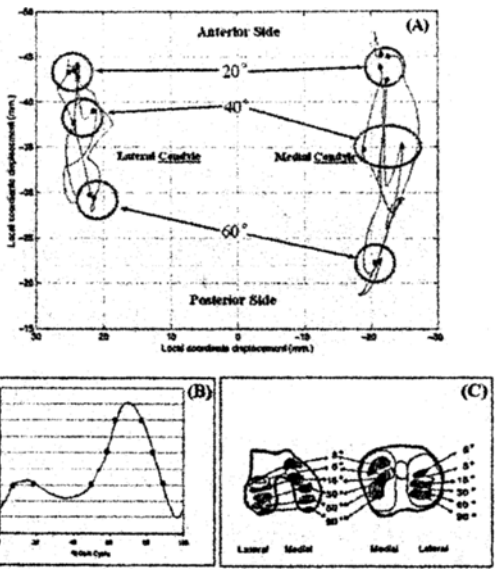

Fig. 8 (a) Tibio-femoral joint-articulating surface motion during human gait using improved kinematic contact model, (b) Flexion/Extension rotation angles during one gait cycle, (c) Tibio-femoral contact area (scanned picture from Iseki et al., 1976)

$\mathbf{F}^{Lc}$ and $\mathbf{F}^{Mc}$ can be solved simultaneously.

$$\begin{bmatrix} a_{11} & a_{12} \\ a_{21} & a_{22} \end{bmatrix} \begin{Bmatrix} \mathbf{F}^{Lc} \\ \mathbf{F}^{Mc} \end{Bmatrix} = \begin{bmatrix} b_1 \\ b_2 \end{bmatrix} \tag{32}$$

where

$$a_{11} = 1 + (\tilde{\mathbf{r}}^L \hat{\mathbf{n}}^L)^T (\tilde{\mathbf{r}}^L \hat{\mathbf{n}}^L) \tag{33}$$

$$a_{12} = (\hat{\mathbf{n}}^M)^T \hat{\mathbf{n}}^L + (\tilde{\mathbf{r}}^M \hat{\mathbf{n}}^M)^T (\tilde{\mathbf{r}}^L \hat{\mathbf{n}}^L) \tag{34}$$

$$a_{21} = 1 + (\tilde{\mathbf{r}}^M \hat{\mathbf{n}}^M)^T (\tilde{\mathbf{r}}^M \hat{\mathbf{n}}^M) \tag{35}$$

$$a_{22} = (\hat{\mathbf{n}}^L)^T \hat{\mathbf{n}}^M + (\tilde{\mathbf{r}}^L \hat{\mathbf{n}}^L)^T (\tilde{\mathbf{r}}^M \hat{\mathbf{n}}^M) \tag{36}$$

$$b_1 = -\sum_{i=1}^{12} (\mathbf{F}^{Ligai})^T \hat{\mathbf{n}}^L + \mathbf{F}^{*T} \hat{\mathbf{n}}^L - \sum_{i=1}^{12} (\tilde{\mathbf{r}}_i \mathbf{F}^{Ligai})^T (\tilde{\mathbf{r}}^L \mathbf{n}^L) + \mathbf{m}^{*T} (\tilde{\mathbf{r}}^L \hat{\mathbf{n}}^L) \tag{37}$$

$$b_2 = -\sum_{i=1}^{12} (\mathbf{F}^{Ligai})^T \hat{\mathbf{n}}^M + \mathbf{F}^{*T} \hat{\mathbf{n}}^M - \sum_{i=1}^{12} (\tilde{\mathbf{r}}_i \mathbf{F}^{Ligai})^T (\tilde{\mathbf{r}}^M \mathbf{n}^M) + \mathbf{m}^{*T} (\tilde{\mathbf{r}}^M \hat{\mathbf{n}}^M) \tag{38}$$

While the knee joint model introduced in this paper characterizes 6 DOF motion with ligamentous articulation, we believe our kinetic model yields a relatively simple solution that lends itself to computational implementation.

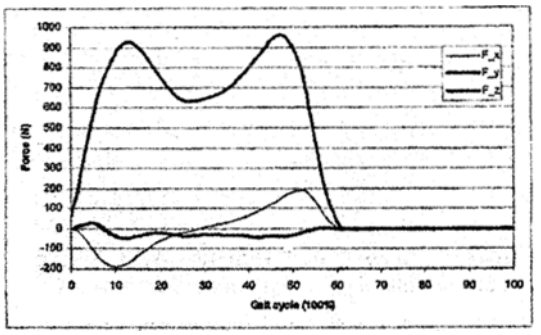

Fig. 9 Force plot of the force plate

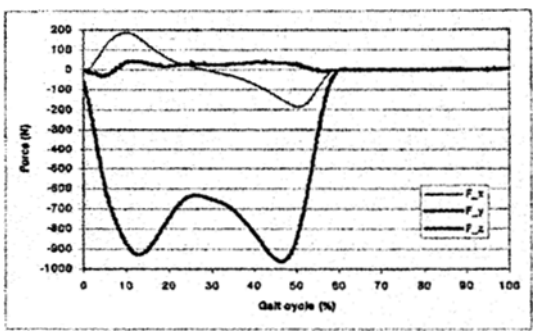

Fig. 10 Internal total reaction force of the knee joint

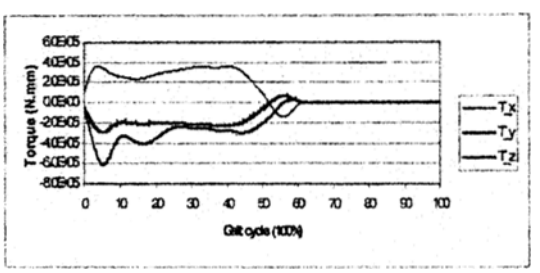

Fig. 11 Internal total reaction torque of knee joint

The external force measured from the force plate during one gait cycle is given in Fig. 9. In the Figure, the sign of the forward direction force F_x is changed during the calibration phase because it represents the hill-contact through toe-off stage. F_y represents the vertical direction force that is mostly affected by body weight. F_z undergoes almost zero force through the entire gait cycle. The total internal force and torque at the knee joint are presented in Figs. 10 and 11. The shape and values of the recovered internal reaction forces are similar to Fig. 9 because the inertia force of each segment is small in the system.

3. Model Validation and Results

In order to verify the developed computational model with respect to kinematic analysis, the contact points between femoral condyle (lateral and medical condyle) and tibia surface are calculated and compared with the previous experimental data, Fig. 8(c). In Fig. 8(a), contact position vector between femoral condyle, lateral and medial side, and tibia plateau on the tibia surface are presented with respect to local coordinate system. The relative motions between the femur and tibia segments using Grood-Suntay's coordinate (Grood and Suntay, 1983) in terms of flexion/extension rotation is shown in Fig. 8(b). As shown in Fig. 8(a), the contact point undergoes sliding and rolling during one gait cycle. In addition, femur and tibia undergo four times 20 degree angles of flexion/extension during one gait cycle, two times 40 degree and 60 degree as well is presented in Fig. 8(b). Thus, these corresponding frames are plotted, black round type dot, on top of the sliding and rolling motion of the knee joint during gait cycle as shown in Fig. 8(a). As observed in the previous studies (Iseki et al., 1976; Bronzino, 1995; Wretenberg et al., 2002), the contact point between femur and tibia moves from anterior side to posterior side as the knee undergoes flexion, reflecting the coupling of anterior and posterior motion with flexion/extension. Also, the contact area of the medial condyle on the tibia plateaus becomes larger than that of the lateral condyle during one gait cycle (Iseki et al., 1976). The anterior/posterior displacement of the contact point on the tibia plateau during one gait cycle is about 16 mm. for the lateral condyle and 25 mm. for the medial condyle. Also, the femur motion on the tibia undergoes lateral/medial movement about 7 mm. and 10 mm. during one gait cycle for the lateral condyle and medial condyle, respectively. Thus, the developed kinematic model, Fig. 8(a) has been verified by the comparison of the previous experimental results, Fig. 8(c), and it is obvious that a fixed-point contact model using spherical joint or universal joint type cannot represent the knee motion properly.

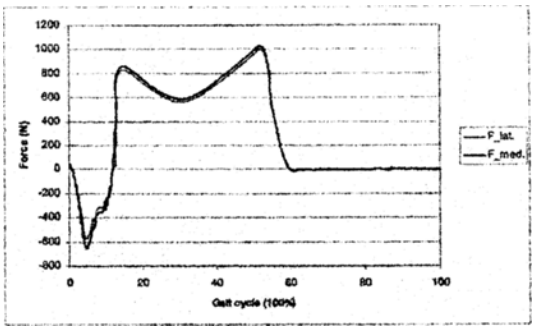

Fig. 12 The lateral and medial contact force of the knee joint

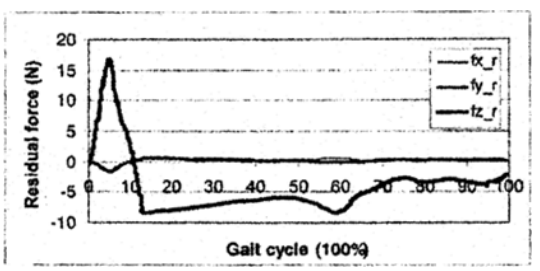

Fig. 13 The absolute residual force plot

Solving Eq. (32) to determine the unknown contact force of the lateral condyle and the medial condyle, the result is given in Fig. 12. In the figure the total internal force in the range of 0~12% of one gait cycle is negative values because the patella, muscles and tendon are not considered in the developed model. Following the results it is believed that the patella, muscles and tendon affect a lot for the internal reaction forces at the initial heel contact stage. In addition, the medial side contact force is larger than that of the lateral side contact force in the knee joint during normal human walking as given in Fig. 12. The total internal force results of the knee joint are reasonably agree well compared to previous studies (Pandy et al., 1988; Koopman et al., 1995).

In order to evaluate the accuracy of the results of our least square method calculating the contact forces at the tibiofemoral joint, the residual terms described in the Eq. (19) are calculated and shown in Fig. 13 through 16. The absolute residual force values are small as shown in

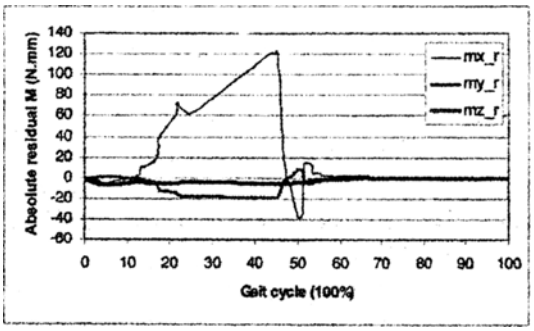

Fig. 14 The absolute residual moment plot

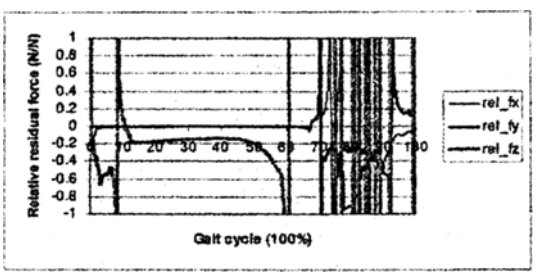

Fig. 15 The relative residual force plot

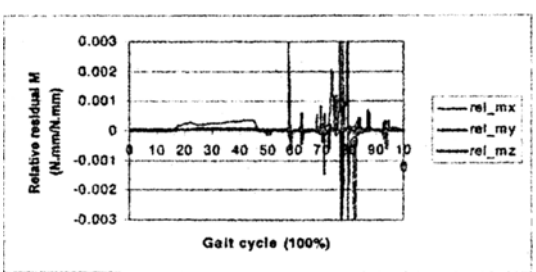

Fig. 16 The relative residual moment plot

Fig. 13. However, there exists a large value for the x-component of the absolute residual moment as shown in Fig. 14 because the developed computational model is not a complete knee joint model. In this model, the forces are in the X-Y plane. Thus, the out of plane moment is ignored.

The relative residuals are calculated as

$$\text{Relative residual force}=\frac{\mathbf{F}-\mathbf{F}^*}{\mathbf{F}^*} \tag{39}$$

$$\text{Relative residual moment}=\frac{\mathbf{M}-\mathbf{M}^*}{\mathbf{M}^*} \tag{40}$$

where, $\mathbf{F}^*$ and $\mathbf{M}^*$ are the total force and moment at the knee joint recovered from the quasi-static solution of the free-body diagram. The contact forces, $\mathbf{F}$ and $\mathbf{M}$ are given in Eqs. (20) and (22), respectively. The relative residual values are presented in Fig. 15 and 16. Following the Figures, the results are reasonably acceptable during the stance phase. However, there exist large values during the swing phase because the residual forces are divided by small calculated reaction forces as described in Eqs. (39) and (40). Thus, the results of the swing phase are ignored.

4. Discussion

Several limitations in our computational model and the invoked assumptions need to be discussed. The developed computational model is composed of two rigid segments such as femur and tibia and twelve ligaments represented by nonlinear spring elements. On the stance phase of the gait, muscle effects are not considered in the developed model since material properties of muscles acting during gait is not well known. In addition representative geometry of the lateral and medial condyles, and ligament origin and insertion position are employed. Furthermore femur and tibia segments are assumed to be homogenous bodies for the calculation of polar moment of inertia since mass density of human segment is not well known.

In the future study, the developed computational model needs to be validated by the comparison with experimental results. In addition, since accurate geometry of femoral and tibia condyles do major role to develop valuable computational model, the 3D geometry model using interpolation method such as Non-Uniform spline Rational B-surfaces is recommended for the future study. Furthermore, accurate ligament origin and insertion position for the experimental subject should be determined to have more meaningful results of ligament function.

Acknowledgment

This study was supported by a grant of the Korea Health 21 R&D Project, Ministry of Health

& Welfare, Republic of Korea. (02-PJ3-PG6-EV06-0002)

References

Abdel-Rahman, E. M. and Hefzy, M. S., 1998, "Three-Dimensional Dynamic Behavior of the Human Knee Joint under Impact Loading," *Medical Engng. & Physics*, Vol. 20, pp. 276~290.

Allard, P., Stokes, I. A. F. and Blanchi, J.-P., 1995, Three-Dimensional Analysis of Human Movement, Human Kinetics, Champaign, Illinois.

Ateshian, G. A., Lai, W. M., Zhu, W. B. and Mow, V. C., 1994, "An Asymptotic Solution for the Contact of Two Biphasic Cartilage Layers," *J. Biomechanics*, Vol. 27, pp. 1347~1360.

Attfield, S. F., Gleeson, N. P., Pickering, P. and Rees, D., 1998, "Evaluation of Dynamic Anterior Cruciate Ligaments Strain During Ambulation," *Gait & Posture*, Vol. 7, pp. 154~155.

Bronzino, J. D., 1995, The Biomedical Engineering Handbook, Boca Raton; CRC Press; IEEE Press.

Brown, T. D. and Shaw, D. T., 1984, In-Vitro Contact Stress Distributions on the Femoral Condyles, *J. orthopedic research society*, Vol. 2, No. 2.

Bobbert, M. F., Schamhardt, H. C. and Nigg, B. M., 1991, "Calculation of Vertical Ground Reaction Force Estimates During Running from Position Data," *J. Biomechanics*, Vol. 24, No. 12, pp. 1095~1105.

Eberhardt, A. W., Keer, L. M., Lewis, J. L. and Vithoontien, V., 1990, "An Analytical Model of Joint Contact," *J. Biomech. Engng.*, Vol. 112, pp. 407~413.

Eberhardt, A. W., Lewis, J. L. and Keer, L. M., 1991, "Contact of Layered Elastic Spheres as a Model of Joint Contact: Effect of Tangential Load and Friction," *J. Biomech. Engng.*, Vol. 113, pp. 107~108.

Grood, E. S. and Suntay, W. J., 1983, "A Joint Coordinate System for the Clinical Description of Three-Dimensional Motions: Application to the Knee," *Journal of Biomechanical Engineering*, Vol. 105, pp. 136~144.

Iseki, F. and Tomatsu, T., 1976, "The Biomechanics of the Knee Joint with Special Reference to the Contact Area," *Keio J. Med.* Vol. 25, pp. 37~44.

Kadaba, M. P., Ramakrishan, H. K. and Wootten, M. E., 1990, "Measurement of Lower Extremity Kinematics During Level Walking," *Journal of Orthopaedic Research Society*, Vol. 8, No. 3, pp. 383~392.

Kapandji, I. A., 1970, The Physiology of the Joint: Volume Two Lower Lim, Churchill Livingston Inc., New York.

Koopman, B., Grootenboer, H. J. and Jongh, H. J. de, 1995, An Inverse Dynamic Model for the Analysis, Reconstruction and Prediction of Bipedal Walking, J. Biomechanics, Vol. 28, No. 11, pp. 1369~1376.

Mun, J. H., 2001, "A New Experimental Error Reduction Method for Three-Dimensional Human Motion Analysis," *Journal of Biomedical Engineering Research*, Vol. 22, pp. 459~467.

Mun, J. H. and Takeuchi, S., 2002, "Three-Dimensional Kinematic Model of the Human Knee Joint During Gait," *Journal of Biomedical Engineering Research*, Vol. 23, pp. 171~179.

Pandy, M. G. and Berme N., 1988, A Numerical Method for Simulating the Dynamics of Human Walking, *J. Biomechanics*, Vol. 21, No. 12, pp. 1043~1051.

Reinschmidt, C., Bobert, A. J. van den, Lundberg, A., Nigg, B. M., Murphy, N., Stacoff, A. and Stano, A., 1997, "Tibiofemoral and Tibiocalcaneal Motion During Walking: External vs. Skeletal Marker," *Gait and Posture*, Vol. 6, pp. 98~109.

Wilson, D. R. and O'Connor, J. J., 1997, "A Three-Dimensional Geometric Model of the Knee for the Study of Joint Forces in Gait," *Gait & Posture*, Vol. 5, pp. 108~115.

Wretenberg, P., Ramsey, D. K., Nemeth, G., 2002, "Tibiofemoral Contact Points Relative to Flexion Angle Measured with MRI," *Clinical Biomechancis*, Vol. 17, pp. 477~485.

Zwick, E. B., Saraph, V., Zwick, G, Steinwender, C., Linhart, W. E. and Steinwender, G., 2002, "Medial Hamstring Lengthening in the Presence of Hip Flexor Tightness in Spastic Dipegia," *Gait & Posture*, Vol. 16, pp. 288~296.